Crystallography of the (3×3) surface reconstruction of $3C$-SiC(111), $4H$-SiC(0001), and $6H$-SiC(0001) surfaces retrieved by low-energy electron diffraction

J. Schardt, J. Bernhardt, U. Starke,* and K. Heinz
Lehrstuhl für Festkörperphysik, Universität Erlangen-Nürnberg, Staudtstrasse 7, D-91058 Erlangen, Germany
(Received 12 May 2000)

The drastic (3×3) reconstruction of $3C$-SiC(111) is crystallographically determined by joint application of quantitative low-energy electron diffraction and holographic interpretation of diffraction intensities, scanning tunneling microscopy, and Auger electron spectroscopy. The reconstruction is shown to be present also on the $4H$- and $6H$-SiC(0001) surfaces, i.e., to be largely independent of the SiC polytype. It corresponds to a new type of semiconductor $(n\times n)$ surface restructuring characterized by a considerable reduction of surface dangling bonds. This is equivalent to a very effective passivation of the surfaces, favoring crystal growth by a step flow mechanism.

I. SURFACE RECONSTRUCTION AND CRYSTAL GROWTH OF SIC

Rather as a rule than an exception, semiconductor surfaces exhibit complex surface atomic structures, which can be very different from the bulklike termination geometry. This is due to the truncation of strong and covalent chemical bonds upon which surface atoms start to rearrange in order to find a new equilibrium state with the number of dangling bonds minimized. Not surprisingly, this reconstructed surface dominates the surface properties that determine the solid's interaction with the outside world. In particular, as crystal growth proceeds via the surface, the reconstruction should affect any growth process. In fact, growth of silicon carbide (SiC) is the background and motivation of the present paper, which deals with the (3×3) reconstruction of (111) and (0001) surfaces of this material. SiC is interesting because of its unique electronic properties[1] and is on its way to becoming an important material for electronic devices. Yet, as it exists in many polytypes,[2] the development of high-quality crystalline samples is difficult and can only be achieved through special techniques. One of them is *step-controlled homoepitaxy* by chemical vapor deposition (CVD) of the material on an off-oriented seed crystal (for a review, see Ref. 3). The off orientation is equivalent to the presence of surface steps, which appear in units of Si-C bilayers containing one sublayer each of silicon and carbon. As the polytypism mentioned is characterized by the stacking sequence of these bilayers,[2] the polytype of the seed crystal is exposed at the steps. So adatoms arriving on a terrace and capable to migrate to steps can easily copy the stacking sequence. This corresponds to a step flow mechanism which facilitates the homoepitaxial growth of a given single polytype material.[3]

Interestingly, it became evident by use of reflection high-energy electron diffraction during both gas-source and solid-source molecular beam epitaxy (MBE) that the step flow growth is accompanied by the above mentioned (3×3) reconstruction of the terraces.[4–6] It was suggested that the (3×3) surface phase enhances the surface mobility of the impinging adatoms, so that they are not trapped on the terrace (due to largely missing dangling bonds) but can reach the steps to allow for polytype-preserving crystal growth. The material growth by MBE was suggested to take place in two steps by the alternate supply of silicon and carbon, switching periodically between more Si-rich and less Si-rich superstructures, confirmed by joint experimental and theoretical work.[7] This corroborates in a concrete way the above mentioned importance of surface reconstruction with respect to crystal growth. The (3×3) phase of SiC(111) has been shown recently to be characterized by a massive surface reconstruction with a simultaneous reduction of surface dangling bonds by a factor of 9 compared to the bulk truncated surface.[8] This was retrieved experimentally by structure determination using quantitative low-energy electron diffraction (LEED) combined with scanning tunneling microscopy (STM) as well as theoretically by surface energy minimization applying density functional theory (DFT). As the crystallographic details given in this earlier paper had to be rather limited because of space restrictions,[8] we present the full structure in the present paper. Additionally, we describe in some detail the structure determination procedure using quantitative LEED and STM, in particular as this was exceptionally demanding because of the initially unknown type of structural model and the large number of parameters involved. Last but not least, we extended our original investigations of the (3×3) reconstruction of $3C$-SiC(111) to the equivalent reconstruction phases of the polytypes $4H$- and $6H$-SiC(0001).

II. EXPERIMENTAL AND COMPUTATIONAL DETAILS

A. Sample preparation and experimental findings

The samples used were epitaxial CVD grown crystalline films[9,10] obtained from IMC company (Kista, Sweden). The $3C$-SiC(111) sample consisted of a 2 μm thick film grown on a Si(111) surface, while the $4H$- and $6H$-SiC(0001) films were the result of homoepitaxial growth on $4H$- and $6H$-SiC(0001) wafers grown by the modified Lely method.[11] The surfaces were treated *ex situ* in trichloroethylene, acetone, and methanol in order to remove organic impurities, followed by an etching step for the removal of native oxide using HF buffered with NH_4F to $p\mathrm{H}=5$. Then the samples

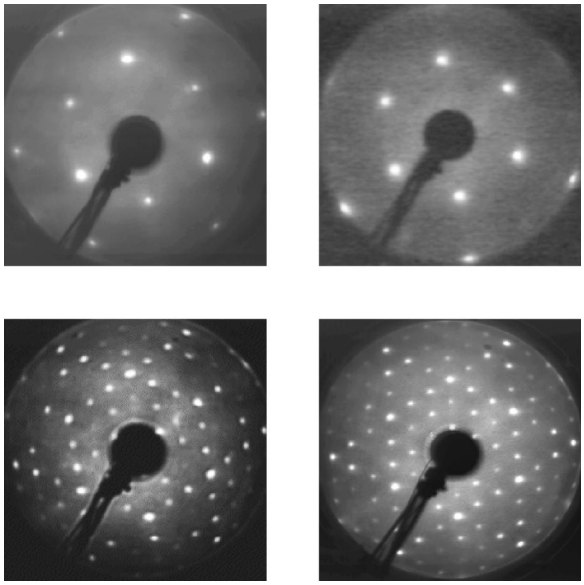

FIG. 1. Left: LEED patterns of the (1×1) (top, 120 eV) and (3×3) (bottom, 134 eV) phases of $3C$-SiC(111). Right: The same for $4H$-SiC(0001) [top: (1×1) at 120 eV, bottom: (3×3) at 135 eV].

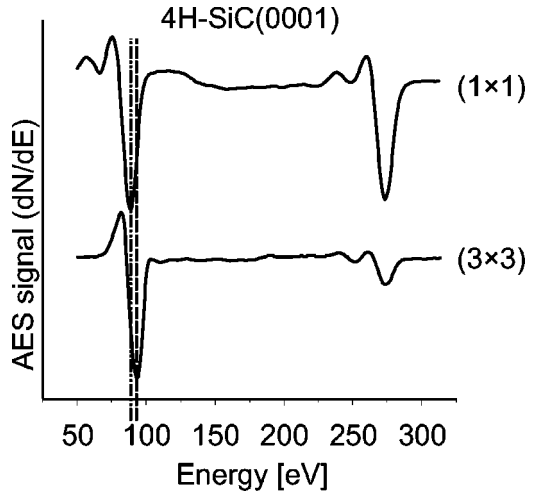

FIG. 2. Auger electron spectra for a (1×1) and a (3×3) phase on $4H$-SiC(0001), displayed as the energy derivative dN/dE. The energy positions of the Si peak minimum are indicated by the dash-dotted line for the (1×1) phase (88 eV) and by the dashed line for the (3×3) phase (92 eV).

were introduced into a home-made ultrahigh vacuum (UHV) vessel supplied with a hemispheric analyzer (CLAM) for Auger electron spectroscopy (AES) and a back-view LEED optics from which *in situ* transfer to a beetle-type STM stage was possible. Immediately after introduction into the UHV, the samples exhibited clear (1×1) LEED patterns, which were of threefold and sixfold rotational symmetry for the cubic and hexagonal samples, respectively, as displayed in Fig. 1 [see Ref. 12 for preparation and structure of the (1×1)-SiC surfaces]. For the hexagonal samples the (3×3) reconstruction resulted from additional silicon flux supplied to the (1×1) surface under simultaneous annealing at about 800 °C. The same (3×3) phase could be produced after transition of the surface through other reconstructed phases,[13] namely, a $(\sqrt{3}\times\sqrt{3})R30°$ reconstruction upon annealing at 950 °C and a $(6\sqrt{3}\times6\sqrt{3})R30°$ phase after further annealing at about 1100 °C. Subsequent recovery of the (3×3) phase again required heating in Si flux, which seems to be necessary to overcompensate the loss of Si during annealing at elevated temperatures. The (3×3)-reconstructed phases of the various samples appear to be silicon rich as evident from the Si/C ratio of the low-energy Auger peaks, which is about a factor 3–4 higher than for the unreconstructed surfaces (see Fig. 2). Such silicon-rich conditions were already found to be essential for the development of the (3×3) phase in earlier work.[14–16] As also shown in Fig. 2, we find that the position of the Si Auger peak (given by the minimum of the differentiated signal) shifts from about 88 eV for the unreconstructed phase to about 92 eV in the case of the (3×3) reconstruction, thus indicating that Si-Si bonds rather than Si-C bonds dominate in the reconstructed surface. It should be noted that Kaplan deduced the presence of a rather continuous Si layer from the additional observation of a surface plasmon at an energy typical for Si.[14] No traces of other elements show up in AES, so the reconstruction seems not to be induced or stabilized by impurities. On the $3C$ sample the extra deposition of silicon was not necessary to produce the (3×3) reconstruction; simple annealing of the (1×1) phase at about 950 °C for 5 min proved to be sufficient. Obviously, silicon enrichment at the reconstructed surface in this case results from diffusion of silicon from the substrate. This intrinsic Si supply also inhibited the development of the other Si-depleted reconstruction phases on our $3C$-SiC sample.

LEED intensity spectra were taken for the (3×3) diffraction spots of all types of samples, for which a computer-controlled and video-based measurement technique was used operating from outside the UHV.[17,18] The measurements were performed at a sample temperature of about 90 K (except for the $6H$ sample, which was investigated at room temperature as its data did not enter the calculation procedure) and at normal incidence of the primary beam as adjusted by comparison of symmetrically equivalent beams. Data collection was in the energy range 40–500 eV. The reliability of the measurement was judged by comparison of spectra of symmetrically equivalent beams and of spectra of identical beams measured from different and differently prepared samples. As a quantitative measure for comparison, the Pendry R factor[19] was used. For samples of identical polytype the R factors were typically below $R=0.1$ for integer as well as fractional order beams, indicating a high level of reliability of the measurement. Eventually, symmetrically equivalent beam spectra were averaged in order to improve the signal-to-noise ratio, to reduce errors caused by residual sample misalignment, and to compensate for possible inhomogeneities in the luminescent LEED screen. All spectra were normalized with respect to the (energy dependent) primary beam current, which was measured simultaneously. The average intensity level of fractional order beams is rather high, indicative of a strong reconstruction. So for the $3C$-(3×3) phase the ratio r_I between fractional and integer order beams averaged in the energy range 50–230 eV (the range of the intensity analysis; see below) is $r_I=0.40$. A judgment of the potential difference of the (3×3) structures on different polytypes can be made from a comparison of the

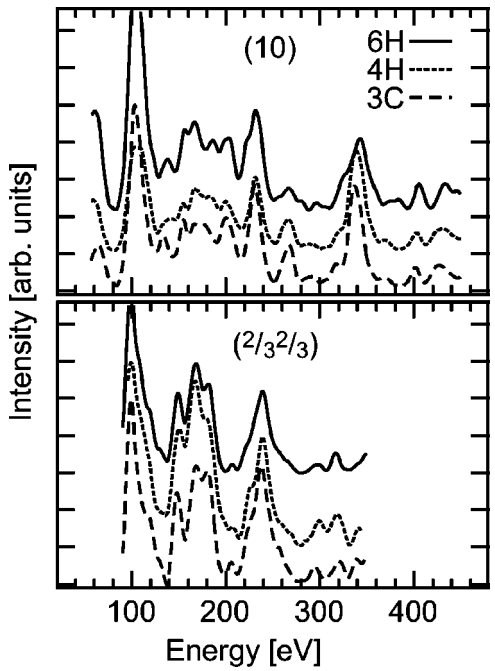

FIG. 3. Comparison of LEED spectra of the (10) and (2/3 2/3) beams (top and bottom panels, respectively) for the (3×3) reconstructions of the 3*C*-(111), 4*H*-(0001), and 6*H*-(0001) surfaces of SiC. Note that (10) and (01) beams were averaged in the case of 3*C*-SiC in order to allow for comparison with the sixfold degenerate beams of the hexagonal samples.

corresponding intensity spectra as displayed in Fig. 3 for selected beams. Given that SiC bilayers below the reconstructed surface slab are differently stacked for the different polytypes, the spectra compare rather well, i.e., the *R* factors between spectra of different surfaces averaged over all available beams are around 0.25. Thus the reconstructions of the three types of surface, must be very similar (though not necessarily strictly identical). Additionally, the thickness of the reconstructed slab together with the first SiC bilayer appears to be large enough that the different stacking of bilayers below has only a little influence on the spectra due to electron attenuation. Therefore, we restricted the quantitative intensity analysis presented below to only one of the surfaces. We chose the 3*C*-SiC(111) surface, as bilayers are uniformly stacked in this sample, so that no different surface domains resulting from different terminations of the unreconstructed surface need to be considered.[12,13]

STM images of the (3×3) reconstruction were acquired on a 4*H*-SiC(0001) surface. As demonstrated in Fig. 4 there is only a single atomic protrusion per (3×3) unit cell. Such STM images have also been published earlier.[13,15,16] They all show this single protrusion per unit cell, independent of the value and polarity of the tunneling voltage applied. This implies that one prominent feature exists in the (3×3) unit cell, a fact that is useful in narrowing down the selection of possible models as elaborated in Sec. III.

B. Computational details

For the surface structure determination the experimental intensities were compared to theoretical spectra for plausible model structures that appear to be compatible with the experimental information from AES, STM, and LEED. The calculation of the intensities was performed by application of full dynamical scattering theory[20,21] and the perturbation method tensor LEED (TLEED).[22,23] The latter allows for easy and fast variation of structural parameters around the values of a prechosen reference structure, for which intensities are calculated fully dynamically. In order to limit the computational effort, the maximum energy in the calculations was restricted to 230 eV, resulting in a total energy width of the data base of $\Delta E = 2253$ eV (396 eV for integer and 1857 eV for fractional order beams). A maximum of nine relativistically calculated and spin averaged phase shifts ($l_{max} = 8$) proved to be sufficient to describe the scattering of both Si and C atoms. They were corrected for (isotropic) thermal vibrations which for bulklike atoms were fixed at root mean square amplitudes of 0.07 Å and 0.10 Å for Si and C atoms according to the Debye temperatures of 750 K and 860 K, respectively, as determined in earlier work on nonreconstructed SiC surfaces.[24] Vibrational parameters for atoms near the surface were treated as fitting parameters for whose variation a modified version of TLEED was used.[25,26] The Si-C bilayers (spacing in the bulk 0.63 Å) and other closely spaced layers (see below) were treated as composite layers with the total layer diffraction matrices calculated in angular momentum representation. Layers were stacked by application of the layer doubling method[20,21] with a maximum of 478 plane waves used. Electron attenuation was simulated by an optical potential $V_{0i} \propto E^{1/3}$ with $V_{0i}(90\ \text{eV}) = 4.0$ eV, as also successful in earlier work. The real part of the inner potential, V_{0r}, was assumed energy independent and treated as a fitting parameter by adjusting the energy scale of calculated and experimental spectra as usual. For the determination of structural parameters an automated search procedure[27] guided by the Pendry *R* factor[19] was used.

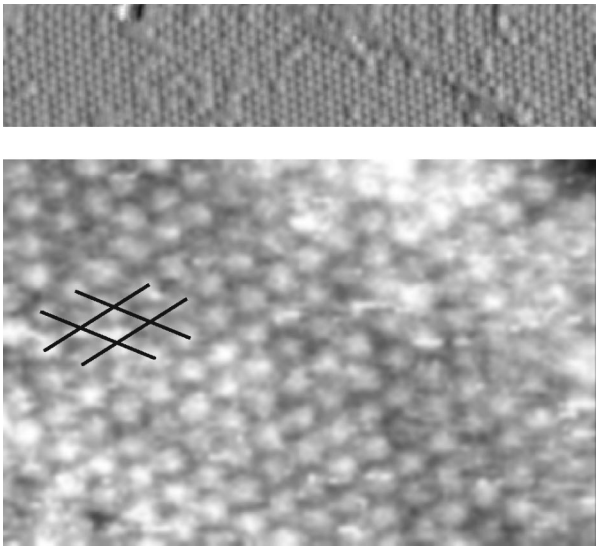

FIG. 4. STM image of 4*H*-SiC(0001)-(3×3) acquired in topographic mode. In the top panel *dz*/*dx* data are displayed suggesting an image illumination from the left (scan area: 501Å×103 Å). The lower panel displays absolute *z* data processed solely by a linear background correction with a (3×3) grid indicated on the left (scan area: 139 Å×101 Å). Tunneling conditions: $U_{tip} = 1.36$ V, $I = 0.4$ nA.

III. TYPE OF STRUCTURAL MODEL

A. Models proposed in the literature

Quantitative surface structure determination by diffraction methods through a trial-and-error procedure to fit the experimental diffraction intensities is always performed in two steps. First, a promising *type* of structural model has to be found, by which structural parameters can be defined. Then, in the second step, the numerical values of these structural parameters must be determined. Certainly, the second step cannot take place before the first one. For complex surface structures this first step is the more difficult the lower the amount of independent information available in addition to the measured diffraction intensities. So, e.g., the full quantitative analysis[28] of possibly the most complex surface structure known in detail today, the (7×7) reconstruction of Si(111), could be achieved by LEED only after key ingredients of this structure [such as the existence of so-called corner holes of dimers, adatoms, and a stacking fault (DAS model)] had been resolved by the previous application of other methods.[29–35] Although the (3×3) unit cell of SiC in the present study is considerably smaller than the (7×7) cell of Si(111), its structure turned out to be complex enough to withstand quantitative solution for a long time because the correct *type* of atomic model was not known.

One should keep in mind that the bulk structure of $3C$-SiC is the same as that of Si except that Si double layers are replaced by Si-C bilayers, of course accompanied by a 20% reduction of the lattice parameter ($a_{3C\text{-SiC}}=4.36$ Å vs $a_{\mathrm{Si}}=5.43$ Å). Now, considering the Si-rich nature of the (3×3) phase one is inclined to assume strong similarities between the Si(111)-(7×7) and SiC(111)-(3×3) reconstructions; in particular because inspection of the model of Si(111)-(7×7) shows that the same type of reconstruction may also develop with any $(2n+1)\times(2n+1)$ periodicity ($n=1,2,\ldots$).[36,37] In fact, periodicities (5×5) and (9×9) (Ref. 38) as well as (11×11) have been found experimentally for Si(111) as metastable phases[39] and even the appearance of single faulted halves of (13×13) unit cells has been reported.[40] So a similar DAS reconstruction seemed to be a good candidate to account also for the (3×3) phase of SiC(111) and, by modifying the stacking in the substrate, for the respective phases of $4H$- and $6H$-SiC(0001). In fact this has been proposed[14] for $3C$-SiC(111)-(3×3), taking into account that by the silicon enrichment the formation of silicon dimers and adatom configurations can easily take place. Figure 5(a) exhibits the corresponding model with unfaulted and faulted halves of the unit cell indicated by light and dark shading, respectively. Evidently, the unit cell contains two adatoms, which should clearly show up in STM images. Yet, as such images exhibit only 1 single protrusion per unit cell[13,15,16] as demonstrated above, this model must be discarded. As a consequence, a variant of the DAS model has been proposed by Kulakov *et al.*[15] with one of the adatoms and its three nearest neighbors as well as the atom directly below removed, so that an atomic hole—in addition to the corner hole—is created as displayed in Fig. 5(b) (Kulakov *et al.* model). Only one of the two possibilities of atom removal is shown (faulted configuration). If atoms in the other half of the unit cell were removed, the adatom tetramer (dark shaded atoms) would be differently oriented (rotation by

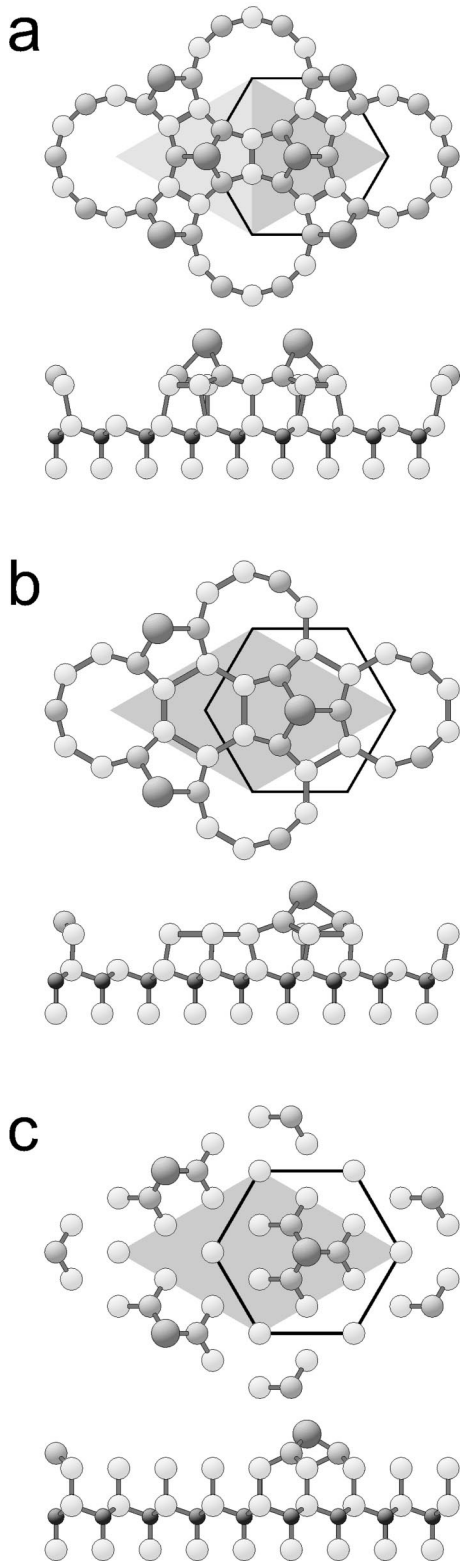

FIG. 5. Model candidates for the (3×3) reconstruction of SiC in on-top and side views with unit cells (shaded) and Wigner-Seitz cells indicated. Small dark spheres (shown only in the side views) represent C atoms, all others Si atoms. The side views enclose part of the substrate and atoms within the unit cell are projected on the $(11\bar{2}0)$ plane. (a) DAS model. (b) Kulakov *et al.* model (Ref. 15). (c) Full Si adlayer (top positions, unrelaxed) + Si adatom cluster (positions from holographic analysis). Note that bonds are not drawn between the Si atoms of the adlayer with a spacing of 3.08 Å.

60°, unfaulted orientation). Of course, with only the protruding atom imaged and not its neighbors below, STM cannot differentiate between the two cases. Based on the observation by STM a further model was suggested by Li and Tsong that consists of isolated tetramers immediately on the SiC substrate;[16] it will be discussed below.

B. Model type selection by holographic LEED, intensity calculations, and STM

The structure of the Kulakov *et al.* model displayed in Fig. 5(b) is rather complex, i.e., the unit cell includes a considerable number of atoms. Therefore, before starting a conventional LEED intensity analysis applying this model we tried to get some additional information about the atomic arrangement in the real surface structure and by that also test the relevancy of the model. Direct, i.e., holographic-type, image reconstruction from the experimental LEED intensities was applied as the STM images clearly show that there is a single adatom per unit cell protruding from the surface. This is a methodical prerequisite of the holographic method as there must be a single distinguished atom to serve as a beam splitter for the incoming primary electron wave. The method was first proposed to work using diffuse LEED intensities[41] and in fact was shown to be successful using such experimental data.[42] The suggestion of application to ordered structures[43,44] as in the present case, i.e., to discrete LEED intensities, was successfully followed in our earlier paper on the present issue.[8] In short, the waves scattered back from the beam splitter atom and forward to the substrate and subsequently backscattered act as reference and object waves, respectively. They interfere to produce the hologram from which the real space image can be reconstructed by a Fourier-like transform. Additional scattering contributions and disturbances by multiple scattering cancel to a certain extent by proper energy averaging included in the transform (for recent reviews, see Refs. 45–47). Using all available LEED intensities in the energy range 50–300 eV (for more details, see Ref. 48) a clearly resolved atomic image results as displayed in Fig. 6 (image data below 25% of the maximum value were interpreted as noise and truncated). Only atoms in the neighborhood of the adatom are reconstructed; more distant ones (in particular in the lateral direction) do not appear because their contribution to the object wave is too small due to electron attenuation and off-normal scattering. The beam splitter atom itself is not reconstructed but defines the origin of the coordinates. It is artificially added in Fig. 6 as a dark sphere and the inset displays all atoms in a ball-and-stick model together with the corresponding interlayer spacings.

Evidently, the atomic cluster determined holographically compares nicely with that around the adatom of the Kulakov *et al.* model in Fig. 5(b). The trimer below the adatom and the two atoms vertically underneath clearly show up. As the orientation of the substrate is known from investigation of the unreconstructed surface,[12,24,49] it is easily possible to identify the cluster as the faulted atomic arrangement. So one is inclined to accept this type of model as the starting structure whose parameters, including the positions of the nonreconstructed atoms in the unit cell, can now be determined or refined in a conventional LEED analysis. Yet the TLEED

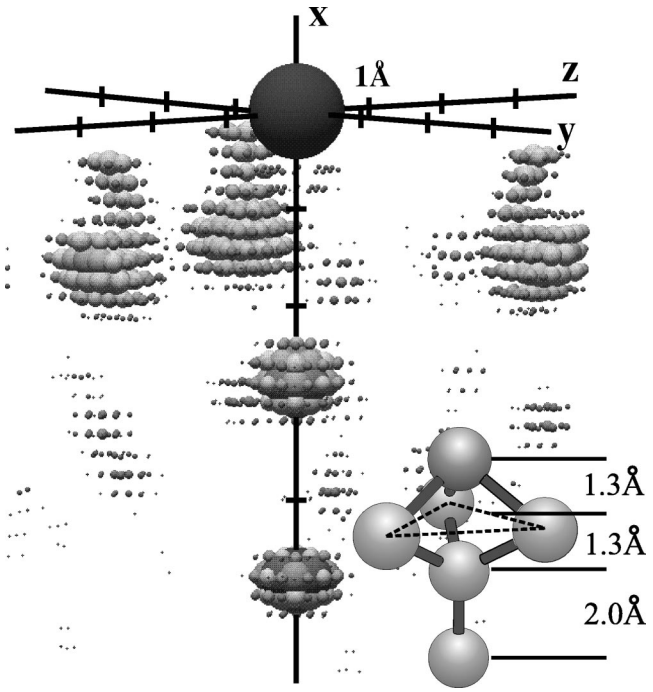

FIG. 6. Three-dimensional real space image of the atomic cluster surrounding the adatom in the (3×3) unit cell of $3C$-SiC(111). The adatom itself (dark sphere) cannot be reconstructed; its position defines the zero of coordinates.

analysis produces a best-fit R factor as high as 0.78, by which the Kulakov model *et al.* must also be ruled out.

At this point reinspection of the STM images and comparison to images available for Si(111)-(7×7) (e.g., Ref. 38) suggest that the structure under investigation exhibits no corner holes as assumed so far. The latter clearly show up for Si(111)-(7×7) but not for SiC-(3×3). In addition, if the diffraction intensities calculated for the Kulakov *et al.* model are used for the holographic image reconstruction, the resulting image suffers from considerable noise and artifacts[48] as opposed to the image based on experimental data displayed above. These disturbances can be interpreted as due to the corner hole being effective as an *additional* beam splitter, so that the prerequisite of a single beam splitter is violated and the reconstructed image must be considerably disturbed as observed.[48] Therefore, the correct model must be characterized by the adatom (or adcluster) being the prominent feature of the reconstruction with corner holes and vacancies absent. The simplest model in this sense is a single adatom in the $T4$ site on the otherwise unreconstructed (or only modestly reconstructed) SiC substrate as found, e.g., for the $4H$-SiC(0001)-$(\sqrt{3}\times\sqrt{3})R30°$ phase.[50] However, this model could not explain the excess amount of Si present on the surface as retrieved from AES and one would not expect a stacking fault in the topmost substrate bilayer. In addition, the atom immediately below the beam splitter must be a carbon atom, which according to recent tests should barely be visible in the image reconstruction due to the much weaker scattering of carbon compared to silicon.[51] Consistently, the best-fit R factor for this model is only 0.69. Also invalidating the model, the calculated ratio of average fractional and integer order beam intensities is only $r_I=0.09$, compared to the experimental value of 0.40. The ratio in-

creases if a full tetramer of atoms (the beam splitter plus the trimer below) is positioned on the SiC substrate as suggested by Li and Tsong.[16] Such a model (with Si constituing the tetramers) would also be more compatible with the Si enrichment observed. However, it is not consistent with the (holographically) reconstructed atomic cluster because in the substrate bilayer there are no two atoms directly below the adatom independent of the position of the tetramer (see Ref. 48 for details). In addition, and not surprisingly, the best-fit R factor is again too high (0.76) to take this model further into account.

As a consequence of all findings retrieved by the various methods applied, i.e., that the surface is silicon rich (AES and Ref. 14), there is a single protruding atom (STM), there is a (known) silicon pentamer below (holographic LEED), there are no corner holes or vacancies (STM), and simple adatom models are ruled out [LEED $I(E)$], we have to return to a more complex type of model, which contains the reconstructed cluster, but has to be considerably modified compared to the model displayed in Fig. 5(b) so that no atomic holes are present. To account for the Si enrichment this requirement could be met by a *full* silicon adlayer on the SiC substrate with the additional tetramer of atoms residing on top of this adlayer. From comparison to the unreconstructed (1×1) surface (see above) the faulted arrangement of the adatom cluster has to be chosen. This situation is sketched in Fig. 5(c). The reconstructed cluster as appearing in Fig. 6 consists of the tetramer and the two (silicon) atoms directly underneath in the adlayer and the first substrate bilayer, respectively. The detailed structure of the adlayer remains to be solved. Clearly, it cannot be a full Si bilayer due to the reduced lattice parameter of SiC. So we start with a Si monolayer as displayed in Fig. 5(c). There the Si atoms are positioned on top of the Si atoms of the topmost SiC bilayer although this still cannot be the final structure as Si atoms are singly bonded to the substrate and 3.08 Å apart. Nevertheless, except for the cluster region, the unit cell is rather flat, so there is no other structural unit acting as an effective beam splitter. Consistently, holographic reconstruction of an image from intensities calculated for such a (not yet optimized) model[48] produces the same atomic cluster as displayed in Fig. 6. Due to the unfavorable bonding situation, considerable atomic relaxation must be expected to take place, i.e., the precise atomic positions of all atoms involved in the surface reconstruction must be determined. For this, conventional LEED intensity analysis was applied as presented in the next section.

IV. STRUCTURAL PARAMETER DETERMINATION

In the structural model evolving from the discussion so far [Fig. 5(c)], the atomic slab above the substrate consists of 13 atoms per (3×3) unit cell, i.e., nine atoms in the silicon adlayer and four atoms in the tetramer. As outlined above the analysis has to optimize the positions of the Si adlayer atoms (bonding situation). However, it will also have to include the atoms whose positions were holographically determined because the accuracy of this procedure is of the order of 0.5 Å only, i.e., insufficient with respect to the standards of today's surface crystallography. Equivalently, the model drawn in Fig. 5(c) does not yield a satisfying fit between experimental

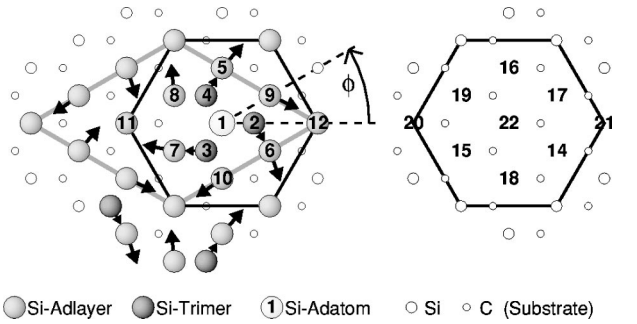

FIG. 7. Model according to Fig. 5(c) with atoms numbered for reference in the text (atom no. 13 is below atom no. 1). Unit cell and Wigner-Seitz cell are indicated by gray and black lines, respectively. On the right side atomic numbers are given for the topmost substrate layer with a translated Wigner-Seitz cell indicating the position with respect to the adlayer atoms on the left. Arrows indicate relaxational movements of the adlayer atoms off the positions in the reference structure. For a cylindrical coordinate representation of the final (optimized) atomic positions (cf. Table I below) the definition of the azimuthal angle ϕ is sketched for the case of atom 9.

and calculated model intensities. As at least the top substrate bilayer must be expected also to reconstruct due to interaction with the slab above, which involves another 18 atoms, there are a total of 31 atoms with not yet or not precisely known positions. Their coordinates together with some nonstructural parameters amount to about 10^2 parameters to be considered in the intensity analysis. Yet, by inspection of the atomic arrangement around the adatom as displayed and numbered in detail in Fig. 7, one notices that certain atoms, namely, of groups (2,3,4), (5,6,7), and (8,9,10), are in equivalent bonding configurations. In fact, all six atoms (5,6,7) and (8,9,10) are equivalent in the unrelaxed structure of Fig. 5(c) according to the mirror plane of the substrate. However, if the displacements allowed in the adlayer include a rotation around the adatom this mirror plane is lost and only threefold rotational symmetry remains, which differentiates these two groups. In effect, we can expect that three coordinates will describe the full group of three atoms in each case due to symmetry constraints. For the same reason only vertical variations should occur for atoms 1,11,12,13, and with the substrate assumed to be bulklike terminated as a first approximation, a total of only $9+4=13$ coordinates remain for the moment. They were used for a first coarse fit using TLEED. For the reference calculation, the structural parameters resulting from the holographic reconstruction were used and an unbuckled adlayer was assumed with positions on top of an ideally arranged Si-C bilayer [Fig. 5(c)]. First, vertical and lateral coordinates were varied separately in subsequent steps. Then, in a next step the silicon atoms of the top substrate bilayer were also allowed to vary with, however, lateral coordinates of all other atoms fixed. The intermediate best-fit R factor resulting by this procedure is $R=0.31$. One important feature of the corresponding structure is that there are pronounced lateral relaxations of atoms in all three groups denoted above, as indicated by the arrows in Fig. 7. These movements are both radial and indeed rotational around the centered adatom (no. 1) with each set of three atoms (from adjacent Wiegner-Seitz cells as drawn in Fig. 7) of groups (5,6,7) and (8,9,10) closing in toward atoms

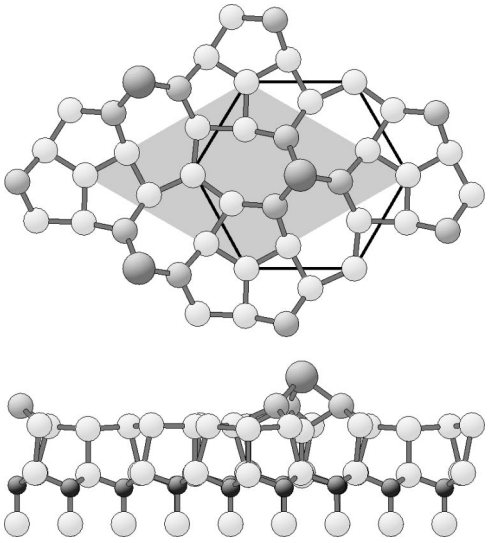

FIG. 8. Top and side views of the optimized twist reconstructed model, drawn in the same style as Fig. 5.

11 and 12, respectively. This obviously takes place to optimize the bonding and coordination in the surface and triggered the name *twist* model that we propose. Note that the crystallographic fit procedure finds these displacements based on the diffraction data alone without any input of bonding, coordination, or energy considerations. Top and side views of the model in its eventual best-fit configuration are displayed in Fig. 8 for comparison to the *untwisted* starting structure [Fig. 5(c)]. It should be noted that the twist rotation may be present clockwise or anticlockwise on the surface, most probably in ordered domains of considerable size. This can be concluded from the absence of any obvious domain boundaries within (3×3) ordered regions in the STM images, as two unit cells of opposite rotational orientation should contain more than one unsaturated bond at their border. Correspondingly, for the fit procedure calculated intensities of both types of domain were averaged, or, technically speaking, beams were averaged according to the original substrate mirror plane. To further underline the significance of the rotational displacements the coupling of the three atomic groups was removed for a test calculation. Then the trend for the rotation could be detected as well, with the atoms moving in a concerted fashion in the same orientational direction.

Although these lateral relaxations undoubtedly take place, as also indicated by the decrease of the *R* factor, the precision of their determination by LEED is limited. This is due to the reduced sensitivity of the intensities for lateral parameters as compared to those normal to the surface—at least for a diffraction geometry as chosen with normal primary beam incidence. An additional factor contributing to this insensitivity certainly is the multidimensionality of the parameter space. We therefore fixed the lateral parameters to values that had resulted from first-principles calculations for $3C$-SiC(111)-(3×3) applying DFT in the local density approximation. These calculations,[7,8] to which the above holographically reconstructed cluster had been input, detected lateral displacements in the Si adlayer of as much as 0.74 Å relative to the on-top positions from Fig. 5(c). The rotation relative to the vertial axis through the adatom is 9.3° for the

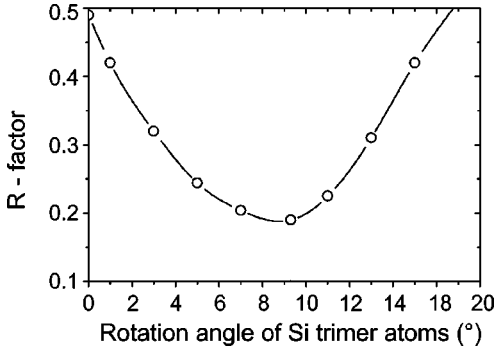

FIG. 9. *R* factor variation with the rotation angle of trimer atoms.

atomic group (2,3,4), 7.4°, for group (5,6,7), and 9.8° for group (8,9,10). Of course, additional buckling displacements were detected, too. Yet, with this DFT determined structure entering the LEED calculation, an *R* factor of only 0.52 results. However, taking this as a reference and allowing for new vertical relaxations and isotropic vibrations of adlayer and adcluster atoms in the TLEED fit procedure, we arrive at a best-fit value of $R=0.19$ with similar values for fractional (0.20) and integer order (0.18) beams and a variance of $\mathrm{var}(R)=0.02$. In order to check the rotation angles, we allowed these to vary, but with all other parameters fixed. Figure 9 demonstrates for the trimer atoms (2,3,4) that the *R*-factor minimum remains at the value given by DFT. As a last check for the validity of the model, the concentration of atoms (11,12) was varied in applying chemical TLEED.[26,52] The best fit was indeed found for a 100% concentration, confirming that no corner holes exist.

The best-fit *R* factor achieved is convincingly low in view of the complexity of the structure. Figure 10 further displays experimental and calculated spectra for two selected beams for visual comparison. Additionally, the ratio between calculated average fractional and integer order beams is $r_I=0.48$ which compares favorably with the experimental value (0.40) in view of the fact that the calculation neglects defects or disordered surface patches. Even the high intensity of the $(\frac{1}{3}0)$ spot [factor of 2.4 with respect to the average intensity of the (10) spot] is almost quantitatively reproduced. The vibrational root mean square amplitudes for the temperature

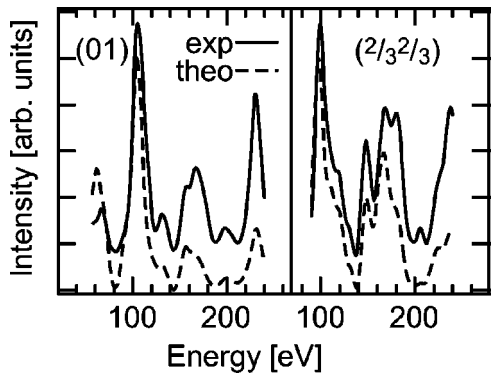

FIG. 10. Experimental (solid lines) and best-fit calculated (dashed lines) spectra for two selected beams (01) and (2/3 2/3) of the $3C$-SiC(111)-(3×3) structure. Note that here the (01) beam is displayed alone, unlike Fig. 3.

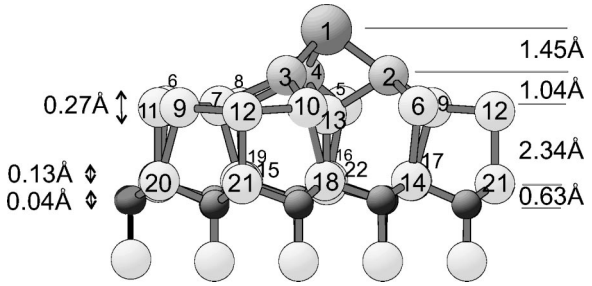

FIG. 11. Vertical cut through the best-fit model. Atomic numbers are consistent with those of Fig. 7 (font size indicating perspective depth). On the right, inter(sub)layer spacings (center of mass planes) are given; the numbers on the left refer to the maximum buckling amplitudes of the respective layers.

of measurement (90 K) are rather high for the protruding adatom and the trimer atoms below (0.27 Å and 0.24 Å, respectively), not unreasonable in view of the bonding situation. With values of 0.12 Å for Si atoms in the adlayer, bulk vibrational amplitudes are approached with increasing depth (0.07 Å and 0.10 Å for Si and C atoms, respectively; cf. Sec. II B).

The main vertical parameters of the model are displayed in Fig. 11 indicated as inter(sub)layer spacings with respect to the center of mass planes and maximum (sub)layer buckling amplitudes. In Table I the cylindrical coordinates of the atoms numbered in Figs. 7 and 11 are given, where the origin refers to the adatom with azimuthal orientation around the surface normal and atom 12 in the 0° position. The definition of the angle ϕ is displayed for the example of atom 9 in Fig. 7. The table also contains angular values ϕ_0 for the original unrelaxed positions [Fig. 5(c)] for comparison as well as the total lateral displacement Δs for each atom. Table II displays the corresponding bond lengths L_{ik} between atoms i and k and the bond angle Φ_{ikj} between the respective atoms. The estimation of the error limits involved is rather difficult because of the many parameters being strongly coupled. Neglecting this coupling, errors for, e.g., adlayer atoms are of the order of ± 0.1 Å for length coordinates and $\pm 2°$ for rotational angles. Of course, with full coupling considered the errors are certainly larger. Yet, as will be discussed in the next section, the structural results retrieved make much sense; in particular, Si-Si chemical bond lengths are very close to what is known from the silicon bulk.

TABLE I. Cylindrical coordinates of atoms numbered in Figs. 7 and 11. The origin $z=r=0$ is positioned at atom no. 1; the azimuthal angle ϕ is given relative to the direction toward atom 12 (see the example given for atom 9 in Fig. 7). For comparison the azimuthal angle ϕ_0 is also given for the unrelaxed position, as well as the lateral displacement due to the twist rotation. Atom groups coupled according to symmetry considerations are represented by their member closest to $\phi=0$. Atoms 1, 13, and 22 being positioned on the origin axis have no azimuthal angle defined as indicated by the dashes in the ϕ columns. Dashes in the Δs column indicate the lateral displacements are frozen due to symmetry constraints of the model.

Atom no. i	z (Å)	r (Å)	ϕ (deg)	ϕ_0 (deg)	Δs (Å)
1	0	0			
2 (3,4)	1.45	2.00	−9.3	0	0.38
6 (5,7)	2.42	3.68	−37.7	−30	0.74
9 (8,10)	2.47	3.60	20.2	30	0.74
11	2.47	5.34	180	180	–
12	2.60	5.34	0	0	–
13	2.69	0	–	–	–
14 (15,16)	4.79	3.12	−28.9	−30	0.06
17 (18,19)	4.80	3.10	31.1	30	0.06
20	4.85	5.34	180	180	–
21	4.89	5.34	0	0	–
22	4.92	0	–	–	–

V. DISCUSSION AND CONCLUSION

The twist reconstruction retrieved is in impressive agreement with results of DFT calculations.[7,8] Compared to an unreconstructed (yet relaxed) $3C$-SiC(111)-(1×1) surface the (3×3) structure yields an energy reduction of as much as 0.91 eV per (1×1) unit cell. The structural parameters determined in the LEED analysis agree favorably with those obtained by the (zero temperature) energy minimization by DFT; deviations are 0.08 Å at maximum for atomic coordi-

TABLE II. Bond lengths L_{ik} between atoms i,k and bond angles Φ_{ijk} between atoms i,k,j according to the numbering given in Figs. 7 and 11.

Atom pairs i,j			L_{ik} (Å)	atoms i,j,k			Φ_{ijk} (deg)
1,2	1,3	1,4	2.47	2,1,3	3,1,4	4,1,2	88.8
2,6	3,7	4,5	2.35	1,2,13	1,3,13	1,4,13	67.9
2,9	3,10	4,8	2.31	6,2,9	7,3,19	5,4,8	97.6
2,13	3,13	4,13	2.35	5,11,6	6,11,7	7,11,5	120.0
5,11	6,11	7,11	2.39	5,11,20	6,11,20	7,11,20	91.3
5,10	6,8	7,9	2.36	8,12,21	9,12,21	10,12,21	93.2
8,12	9,12	10,12	2.35	8,12,9	9,12,10	10,12,8	119.7
5,16	6,14	7,15	2.47				
8,19	9,17	10,18	2.43				
12,21			2.30				
13,22			2.23				
11,20			2.38				

nates. The reconstruction is characterized by a full silicon adlayer on top of the SiC substrate and a single silicon tetramer per unit cell above. Locally, the surface protruding adatom resides in a T_4 site with the trimer in faulted orientation with respect to the atomic stacking below. As a consequence, bonding angles to the trimer adatoms below (88.8°) deviate considerably from the usual tetrahedral bonding situation (109.5°) and bond lengths ($L_{1,2(3)(4)} = 2.47$ Å) are expanded compared to the silicon bulk value (2.35 Å). All silicon atoms in the surface are fourfold coordinated except the adatom at which the only dangling bond in the unit cell is located. The existence of a single dangling bond per unit cell should entail metallic character of the surface. Yet angle-resolved ultraviolet photoelectron spectroscopy and inverse photoelectron spectroscopy experiments reveal that the surface is semiconducting.[56,57] This discrepancy can be resolved in favor of the latter property by inclusion of electron correlations in the DFT calculations.[58] In this context the $(\sqrt{3}\times\sqrt{3})R30°$ phase on the SiC(111)/(0001) surface should be mentioned. There, a T_4 site has also been retrieved using LEED intensities of a $4H$-SiC-$(\sqrt{3}\times\sqrt{3})R30°$ reconstructed surface[50] with very similar bond lengths (2.42–2.47 Å for different domains with different surface terminations of the substrate layer stacking sequence), also in good agreement with first-principles calculations.[53–55] Yet for this surface also an apparent contradiction existed between the semiconducting nature of the $(\sqrt{3}\times\sqrt{3})R30°$ structure found experimentally[59,60] and the single dangling bond per unit cell. The $(\sqrt{3}\times\sqrt{3})R30°$ structure was the first SiC surface phase where this type of problem occurred and it was resolved by considering strong electronic correlation effects.[61]

The adlayer geometry retrieved for the (3×3) phase is nearly planar as can be seen from its small maximum buckling amplitude (0.27 Å). The bond angles between two adlayer atoms and a substrate atom (e.g., $\Phi_{7,11,20}$) are close to 90°, i.e., there is again no ideal tetrahedral bonding as is usually present for Si. Instead, the coordination of, e.g., atoms no. 11 and 12 (which do not coordinate to the trimer that supports the adatom) to their neighbors rotationally is nearly ideally threefold symmetric, as indicated by the respective angles 119.7° and 120.0°, i.e., there is a cloverlike in-plane bonding configuration.[8] For the other atoms in the adlayer the situation is similar. This indicates an sp^2 or $(sp+p)$ hybridization of in-plane orbitals and—in view of the nearly 90° bonding angle to the substrate—p bonding in the vertical direction. Although from the latter circumstance an expanded bond length compared to the value in the silicon bulk should be expected, the deviations of *all* bond lengths from the bulk value are rather small (±0.15 Å; cf. Table I). Certainly, this is due to the fact that all adlayer atoms are fourfold coordinated. Obviously, the reconstruction is driven by dangling bond minimization and bond length optimization so that only bond angles are distorted, although significantly. One should also note that a strong reconstruction should already be expected from the fact that the surface is silicon rich (a ''rough Si monolayer''[7] of 13/9 coverage above the SiC substrate) and that the Si and SiC lattice parameters differ by as much as 20%, so that the considerable surface stress involved should induce reconstruction.

The SiC-(3×3) reconstruction determined corresponds to an $(n\times n)$ semiconductor surface reconstruction that is different from the DAS model holding for Si(111)-$[(2n+1)\times(2n+1)]$ reconstructions and different from the Kulakov *et al.* model in that there are no corner holes or vacancies present. Dangling bond saturation is optimal; only one out of nine dangling bonds per (3×3) cell remains. This is interpreted as allowing for the high mobility of arriving atoms during crystal growth, i.e., for their easy migration to surface steps to copy the underlying polytype by a step flow growth mechanism as discussed in Sec. I. As this picture should be independent of the polytype under consideration, it is additionally supported by our finding that the diffraction intensities of the (3×3) phases of $3C$-, $4H$-, and $6H$-SiC are very similar. The reconstructed surface slab extends rather deep into the surface, from the top adatom down to the first carbon (sub)layer; only below the latter can different bilayer stacking characteristic of the different polytypes develop. From the structural parameters determined we take it that the depth of the slab amounts to about 5.5 Å, so by electron attenuation the influence of the stacking, i.e., of the polytype under consideration, should be rather small—in agreement with the experimental finding and, at least in the end, not surprisingly. Of course, we cannot exclude the possibility that some of the small discrepancies might be due to polytype-specific modifications of the surface reconstruction, but these modifications have to be small.

In conclusion, we have shown that the combined application of different surface sensitive tools, such as quantitative LEED, STM, AES, and holographic LEED in the present case, can resolve complex surface structures even when the type of the correct model is initially unknown. For the densely packed SiC surfaces under consideration, i.e., $3C$-(111) as well as $4H$- and $6H$-(0001), the (3×3) reconstruction investigated is largely independent of the polytype. It corresponds to a type of semiconductor restructuring characterized by a very effective reduction of surface dangling bonds. This passivates the surface considerably so that atoms arriving during crystal growth are not instantly trapped but can find their ideal crystallographic site by diffusion. This corroborates the importance of surface structure and reconstruction for crystal growth.

ACKNOWLEDGMENTS

This work was supported by Deutsche Forschungsgemeinschaft (DFG) through Sonderforschungsbereich 292.

*Corresponding author. Email address: ustarke@fkp.physik.uni-erlangen.de

[1] *Properties of Silicon Carbide*, edited by G.L. Harris EMIS Datareviews Series No. 13 (Inspec, London, 1995).

[2] R. Verma and P. Krishna, *Polymorphism and Polytypism in Crystals* (Wiley, New York, 1966).

[3] T. Kimoto, A. Itoh, and H. Matsunami, Phys. Status Solidi B **202**, 247 (1997).

[4] S. Tanaka, R.S. Kern, and R.F. Davis, Appl. Phys. Lett. **65**, 2851 (1994).

[5] A. Fissel, B. Schröter, and W. Richter, Appl. Phys. Lett. **66**, 3182 (1995).
[6] A. Fissel, K. Pfenninghaus, U. Kaiser, B. Schröter, and W. Richter, Mater. Sci. Eng., B **68**, 1 (1996).
[7] J. Furthmüller, P. Käckel, F. Bechstedt, A. Fissel, K. Pfenninghaus, B. Schröter, and W. Richter, J. Electron. Mater. **27**, 848 (1998).
[8] U. Starke, J. Schardt, J. Bernhardt, M. Franke, K. Reuter, H. Wedler, K. Heinz, J. Furthmüller, P. Käckell, and F. Bechstedt, Phys. Rev. Lett. **80**, 758 (1998).
[9] S. Karmann, W. Suttrop, A. Schöner, M. Schadt, C. Haberstroh, F. Engelbrecht, R. Helbig, and G. Pensl, J. Appl. Phys. **72**, 5437 (1992).
[10] N. Nordell, A. Schöner, and S.G. Andersson, J. Electrochem. Soc. **143**, 2910 (1996).
[11] J.A. Lely, Ber. Dtsch. Keram. Ges. **32**, 229 (1955).
[12] U. Starke, Phys. Status Solidi B **202**, 475 (1997).
[13] U. Starke, J. Schardt, and M. Franke, Appl. Phys. A: Mater. Sci. Process. **65**, 587 (1997).
[14] R. Kaplan, Surf. Sci. **215**, 111 (1989).
[15] M.A. Kulakov, G. Henn, and B. Bullemer, Surf. Sci. **346**, 49 (1996).
[16] L. Li and I.S.T. Tsong, Surf. Sci. **351**, 141 (1996).
[17] K. Heinz and K. Müller, *Structural Studies of Surfaces*, Vol. 91 of *Springer Tracts in Modern Physics*, edited by G. Höhler and E. A. Niekisch (Springer, Berlin, 1982), p. 1.
[18] K. Heinz, Prog. Surf. Sci. **27**, 239 (1988).
[19] J.B. Pendry, J. Phys. C **13**, 937 (1980).
[20] J.B. Pendry, *Low Energy Electron Diffraction* (Academic Press, London, 1974).
[21] M. A. van Hove and S. Y. Tong, *Surface Crystallography by LEED* (Springer, Berlin, 1979).
[22] P.J. Rous, J.B. Pendry, D.K. Saldin, K. Heinz, K. Müller, and N. Bickel, Phys. Rev. Lett. **57**, 2951 (1986).
[23] P.J. Rous, Prog. Surf. Sci. **39**, 3 (1992).
[24] J. Schardt, J. Bernhardt, U. Starke, and K. Heinz, Surf. Rev. Lett. **5**, 181 (1998).
[25] U. Löffler, R. Döll, K. Heinz, and J.B. Pendry, Surf. Sci. **301**, 346 (1994).
[26] K. Heinz, M. Kottcke, U. Löffler, and R. Döll, Surf. Sci. **357-358**, 1 (1996).
[27] M. Kottcke and K. Heinz, Surf. Sci. **376**, 352 (1997).
[28] S.Y. Tong, H. Huang, C.M. Wei, W.E. Packard, F.K. Men, G. Glander, and M.B. Webb, J. Vac. Sci. Technol. A **6**, 615 (1988).
[29] R.J. Culbertson, L.C. Feldman, and P.J. Silverman, Phys. Rev. Lett. **45**, 2043 (1980).
[30] R.M. Tromp, E.J. van Loenen, M. Iwami, and F.W. Saris, Solid State Commun. **44**, 971 (1982).
[31] G. Binnig, H. Rohrer, Ch. Gerber, and E. Weibel, Phys. Rev. Lett. **50**, 120 (1983).
[32] F.J. Himpsel, Phys. Rev. B **27**, 7782 (1983).
[33] E.G. McRae, Phys. Rev. B **28**, 2305 (1983).
[34] P.A. Bennet, L.C. Feldman, Y. Kuk, E.G. McRae, and J.E. Rowe, Phys. Rev. B **28**, 3656 (1983).
[35] K. Takayanagi, Y. Tanishiro, M. Takahashi, and S. Takahashi, J. Vac. Sci. Technol. A **3**, 1502 (1985).
[36] G.-X. Qian and D.J. Chadi, J. Vac. Sci. Technol. B **4**, 1079 (1986).
[37] G.-X. Qian and D.J. Chadi, Phys. Rev. B **35**, 1288 (1987).
[38] R.S. Becker, J.A. Golovchenko, G.S. Higashi, and B.S. Swartzentruber, Phys. Rev. Lett. **57**, 1020 (1986).
[39] Y.-N. Yang and E.D. Williams, Phys. Rev. Lett. **72**, 1862 (1994).
[40] W. Shimada, H. Tochihara, T. Sato, and M. Iwatsuki, Surf. Sci. **423**, L291 (1999).
[41] D.K. Saldin and P.L. de Andres, Phys. Rev. Lett. **64**, 1270 (1990).
[42] C.W. Wei, S.Y. Tong, H. Wedler, M.A. Mendez, and K. Heinz, Phys. Rev. Lett. **72**, 2434 (1994).
[43] M.A. Mendez, C. Glück, and K. Heinz, J. Phys.: Condens. Matter **4**, 999 (1992).
[44] K. Heinz, R. Döll, M. Wagner, U. Löffler, and M.A. Mendez, Appl. Surf. Sci. **70/71**, 367 (1993).
[45] D.K. Saldin, X. Chen, J.A. Vamvakas, M. Ott, H. Wedler, K. Reuter, K. Heinz, and P.L. de Andres, Surf. Rev. Lett. **4**, 991 (1997).
[46] K. Heinz and L. Hammer, Z. Kristallogr. **213**, 615 (1998).
[47] K. Heinz, U. Starke, and J. Bernhardt, Prog. Surf. Sci. **64**, 163 (2000).
[48] K. Reuter, J. Schardt, J. Bernhardt, H. Wedler, U. Starke, and K. Heinz, Phys. Rev. B **58**, 10 806 (1998).
[49] U. Starke, J. Bernhardt, M. Franke, J. Schardt, and K. Heinz, Diamond Relat. Mater. **6**, 1349 (1997).
[50] U. Starke, J. Schardt, J. Bernhardt, M. Fanke, and K. Heinz, Phys. Rev. Lett. **82**, 2107 (1999).
[51] A. Seubert, D.K. Saldin, J. Bernhardt, U. Starke, and K. Heinz, J. Phys.: Condens. Matter **12**, 5527 (2000).
[52] R. Döll, M. Kottcke, and K. Heinz, Phys. Rev. B **48**, 1973 (1993).
[53] J.E. Northrup and J. Neugebauer, Phys. Rev. B **52**, R17 001 (1995).
[54] M. Sabisch, P. Krüger, and J. Pollmann, Phys. Rev. B **55**, 10 561 (1997).
[55] F. Bechstedt, P. Käckell, A. Zywietz, K. Karch, B. Adolph, K. Tenelsen, and J. Furthmüller, Phys. Status Solidi B **202**, 35 (1997).
[56] H. Hüsken, B. Schröter, and W. Richter, Surf. Sci. **407**, L676 (1998).
[57] L.S.O. Johansson, L. Duda, M. Laurenzis, K. Krieftewirth, and B. Reihl, Surf. Sci. **445**, 109 (2000).
[58] J. Furthmüller, F. Bechstedt, H. Hüsken, B. Schröter, and W. Richter, Phys. Rev. B **58**, 13 712 (1998).
[59] L.I. Johansson, F. Owman, and P. Martensson, Surf. Sci. **360**, L478 (1996).
[60] J.-M. Themlin, I. Forbeaux, V. Langlais, H. Belkhiv, and J.-M. Deveben, Europhys. Lett. **39**, 61 (1997).
[61] J.E. Northrup and J. Neugebauer, Phys. Rev. B **57**, R4230 (1998).